TURBULENT SWIRLING FLOW IN 90°-BEND

H. A. ABDALLA*, M. NASR*, B. A. KHALIFA AND W. A. EL-ASKARY*****
Mechanical Power Engineering Department, Faculty of Engineering,
Menoufia University, Shebin EL-Kom, EGYPT
*** Ass. Professor ** Professor *** Graduate Student**

ABSTRACT

An incompressible turbulent-swirling flow through 90 degrees bend with different inlet swirl intensities is predicted by solving the time-average Navier-Stokes equations along with the k-ε turbulence model. The effect of streamline curvature is considered in order to improve the prediction of turbulent-swirling flow in the bend. The inlet swirl velocity profile is close to the solid-body rotation. The effects of swirl intensity, curvature ratio, downstream tangent and Reynolds number on the bend performance are studied. Also, the swirl decay process through the bend is considered. The computational results show that the flow characteristics such as longitudinal, swirl and radial velocities are affected by the inlet swirl intensity. On the other hand, the decay process of swirl is strongly affected by the geometrical parameters and entrance conditions. Also, it is recommended to pass a high turbulent-isothermal fluid without swirl through the bend of shorter downstream tangent and high curvature ratio. An experimental study is carried out to verify the accuracy of the numerical model. In general, the comparisons between the experimental and computational results are in fairly agreement.

Key Words: Swirling Flow, Bend, Flow Characteristics, Turbulent Flow, Performance, Swirling Decay

Manuscript received from Dr: H. A. Abdalla at: 22/ 10/ 1997,
accepted at: 10/ 11/ 1997,
Engineering research bulletin, Vol. 21, No. 1, 1998,
Menoufiya University, Faculty of Engineering,
Shebin El- Kom, Egypt, ISSN. 1110-1180.

1. INTRODUCTION

An important practical case of inlet flow distortion is that of swirling inlet flow. Turbulent swirling flows are found in many internal flow passages, e.g. in flow downstream from a pump or hydraulic turbine. However, the presence of swirling flow is not always beneficial and the designer must either try to remove it or live with its consequences. For example, the flow into an elbow-type draft tube of a water turbine under partial load has a swirling component. The swirl component is the reason for the observed vibration of the draft tube. The objective of this paper was to provide basic information for bends with incompressible swirling inlet flow. In practice, however, flow approaching a bend is not always in a fully developed form, because it depends on the upstream conditions. The flow into the bend may be associated with a swirling motion or shear component in axial velocity. It is possible as a result of fluid machines or spatially curved ducts ahead of the bend.

Few guidelines are available for swirling flow in curved ducts compared with the flow in straight ducts. The velocity distributions across the downstream section of multiple 90 degrees bends were measured by Shimizu[1]. He reported that, depending on the method of connecting the 90 degrees bends upstream, there were various combinations of swirling and axial shear components. These additional flow components may alter the flow pattern from that of the well-known flow in a curved duct. Murakami and Kito[2] analyzed the change of discharge coefficient of 90 degrees elbow flow-meters of circular cross-section due to swirling flow component. Their theoretical study is based on a potential flow model. It showed that even a weak swirling flow (which will be found in the actual pipe lines) has a considerable effect on the discharge coefficient of elbow flow-meter. To verify the theoretical model, they measured the pressures along the convex and concave walls of the bend in the absence and presence of swirl. The results showed that, in the absence of swirl, the pressures along both walls are increased in the region between 20 to 70 degrees from the entrance of the bend. On the other hand, this increase of pressure distributions becomes relatively flat in a swirling flow case. In all cases the pressure on the concave wall is higher than that of the convex wall. Swirling flow of an inviscid fluid through curved pipes was investigated analytically by Kitoh[3]. His results indicated that, when the swirl number of the flow, which is defined as the axial flux of swirl momentum divided by axial momentum times the radius of pipe cross-section, entering the curved bend is large, the flow in the bend is a one-directionally rotative motion. His study showed also that, the angular momentum flux decays in a wavy form along the pipe centerline. When the swirl number was small, a complex secondary flow pattern exists in the cross-stream plane, and the angular momentum flux decay is gradual initially and then drops sharply towards the bend exit. In this case, bend curvature has a significant effect on the flow behavior. Therefore, these results suggested that, swirl effect dominates curved-pipe flows when the swirl number is large. Kitoh and Yu [4] described an approximate viscous solution to the analytical approach, based on

the conservation of angular momentum flux theory of Kitoh [3]. The approximate solution of Kitoh and Yu [4] takes into account the frictional forces on the pipe wall. They calculated the total shear stress as a function of a straight pipe friction coefficient. The study of Kitoh and Yu [4] was aimed to investigate the effect of wall friction on swirling decay in 180 degrees bend with curvature ratio of 0.167. The viscous solution of Kitoh and Yu [4] gave closer agreements with the available experimental data, except in the case of low inlet swirl intensity due to the neglected radial velocity in the equations in this case. Recently, the combined effect of swirl and bend curvature on fully-developed turbulent flow through 180 degrees bend was studied by Anwer and So[5]. In their investigation, mean flow properties, second-order turbulence statistics, wall static pressure and total wall shear stress in the upstream tangent, along 180 degrees bend and in the downstream tangent were measured. The experiments were carried out at one swirl number only; namely swirl number is equal one. These measurements were used to analyze the effect of 180-degrees bend on swirling-turbulent flow. However, their study was concentrated on a single swirl number of one and curvature ratio of 0.077. The results, essentially verified that the secondary motion in the curved pipe is totally re-organized by swirl. Consequently, a more uniform mean flow and turbulence distributions were measured across the curved pipe. The resultant flow becomes fairly symmetric about the pipe axis. So and Anwer [6] extended the previous experimental study of swirling-turbulent flow through a 180-degrees curved bend [5], and its downstream tangent. The extended experimental study was aimed to assess the flow recovery from swirl and bend curvature. They reported that, Dean-cells are absent in the downstream tangent. However, mean flow measurements at 49 pipe diameter downstream of the curved pipe exit showed that, the radial and swirl velocities are identical to that of a fully developed pipe flow. On the other hand, the turbulence field has not completely recovered and takes another 15 pipe diameter before approaching full recovery. Also, the presence of the bend curvature before the pipe flow accelerates swirl decay and significantly shortened the recovery length.

From the previous literature, it is concluded that, few researches were devoted to study the swirl flow throughout 90 degrees bends, [1 and 2]. Also, non of the previous works studied the combined effects of curvature ratios, Reynolds numbers, downstream tangents and swirl intensities on the performance of such bends. In the present work, these effects are studied numerically. The numerical procedure is based on the technique of Patankar[7]. This technique is incorporated with the TEACH computer program[8], which is modified to solve the swirling flow through bends. Furthermore, an experimental study was carried out in the Heat Engine Laboratory, Faculty of Engineering, Menoufia University to verify the computational results. Measurements of static pressure distributions along the concave and convex walls of the bend and its boundary ducts were conducted. Also, the mean longitudinal and swirl velocity profiles across the bend in the plane of curvature

were measured by using a calibrated three-holes probe. The experiments were conducted for various swirl intensities at the bend entrance.

2. NUMERICAL PREDICTIONS

2-1. The Governing Equations and Solution Procedure

The two-dimensional, incompressible, isothermal and turbulent-swirling flows in smooth curved ducts with upstream and downstream straight tangents are assumed in the present work. The turbulent Reynolds equations for conservation of mass, momentum, turbulence energy k and its dissipation rate ε can be written for both cartesian and cylindrical coordinates, in the following general form, Refs. [9] and [10].

$$\frac{1}{y^j}\frac{\partial}{\partial y}\left(\rho y^j v\Phi\right)+\frac{1}{y^j}\frac{\partial}{\partial \theta}(\rho u\Phi)=\frac{1}{y^j}\frac{\partial}{\partial y}\left(\Gamma_\Phi y^j\frac{\partial \Phi}{\partial y}\right)+\frac{1}{y^j}\frac{\partial}{\partial \theta}\left(\Gamma_\Phi\frac{\partial \Phi}{y^j\partial \theta}\right)+S_\Phi \qquad (1)$$

where Φ is a dependent variable (representing 1, u, v, w, k and ε for the conservation of mass, u-momentum, v-momentum, w-momentum, turbulence energy and its dissipation rate, respectively), Γ_Φ is the exchange coefficient, and S_Φ represents the source term. Both Γ_Φ and S_Φ are replaced with suitable terms corresponding to the form Φ takes and are given in Table (1), where certain quantities are defined as follows:

$$G=\mu_t\left[2\left(\frac{1}{y^j}\frac{\partial u}{\partial \theta}+j\frac{v}{y^j}\right)^2+2\left(\frac{\partial v}{\partial y}\right)^2+\left(\frac{1}{y^j}\frac{\partial v}{\partial \theta}+\frac{\partial u}{\partial y}-j\frac{u}{y^j}\right)^2+\left(\frac{1}{y^j}\frac{\partial w}{\partial \theta}\right)^2+\left(\frac{\partial w}{\partial y}\right)^2\right] \qquad (2)$$

$$\mu_{eff}=\mu_\ell+C_\mu\rho\frac{k^2}{\varepsilon} \qquad (3)$$

Conservation of	Φ	Γ_Φ	S_Φ
Continuity	1	0	0
Radial Momentum	v	μ_{eff}	$-\frac{\partial P}{\partial y}+\frac{1}{y^j}\frac{\partial}{\partial y}\left(\mu_t y^j\frac{\partial v}{\partial y}\right)+\frac{1}{y^j}\frac{\partial}{\partial \theta}\left(\mu_t(\frac{\partial u}{\partial y}-j\frac{u}{y^j})\right)$ $+j\left(\frac{\rho u^2}{y^j}-\frac{\mu_{eff}}{y^j}(2\frac{\partial u}{y^j\partial \theta}+\frac{v}{y^j})-\mu_t\frac{v}{y^{2j}}\right)$
Axial Momentum	u	μ_{eff}	$-\frac{1}{y^j}\frac{\partial P}{\partial \theta}+\frac{\partial}{\partial y}\left(\mu_t(\frac{\partial v}{y^j\partial \theta}-j\frac{u}{y^j})\right)+\frac{1}{y^j}\frac{\partial}{\partial \theta}\left(\mu_t(\frac{\partial u}{y^j\partial \theta}+j\frac{2v}{y^j})\right)$ $+j\left(\frac{\mu_{eff}}{y^j}(2\frac{\partial v}{y^j\partial \theta}-\frac{u}{y^j})-\frac{\rho uv}{y^j}+\frac{\mu_t}{y^j}(\frac{\partial u}{\partial y}-\frac{u}{y^j})\right)$
Tangential Momentum	w	μ_{eff}	0
Turbulent Kinetic Energy	k	$\frac{\mu_{eff}}{\sigma_k}$	$G-C_D\rho\varepsilon$
Dissipation Rate of k	ε	$\frac{\mu_{eff}}{\sigma_\varepsilon}$	$\frac{\varepsilon}{k}(C_1G-C_2\rho\varepsilon)$

Table 1. Source Term in the General Equation for Φ, Equation(1)

where,

j = 1, applied to curved duct

j = 0, applied to straight tangent ducts

The standard constants necessary for the turbulence-model are given by Launder and Spalding [11], in Table (2)

C_1	C_2	σ_k	σ_ε	C_D	C_μ
1.44	1.92	1.00	1.30	1.00	0.09

Table 2. The standard Experimental Constants of k-ε Turbulence Model, Ref.[11]

In the present work the effect of streamline curvature has been considered by modifying the value of the constant C_μ on similar lines discussed by Leschziner and Rodi [12]. This could be expressed as:

$$C_\mu = \frac{0.09}{\left[1+0.57j\frac{k^2}{\varepsilon^2}\left(\frac{\partial u}{\partial y}+\frac{u}{y^j}\right)\frac{u}{y^j}\right]} \qquad (4)$$

The solution procedure which uses the finite difference method to solve equation (1) for variable Φ, is a development of Gosman and Pun's [8]. More details about the solution procedure can be found in El-Askary[13]. The converged solutions were accepted when all normalized residuals were less than 0.005. The mesh used was 67×29, with 5 planes along the inlet tangent, 29 planes around 90 degrees bend and the remaining planes in the downstream tangents. The calculation mesh and grid elements are shown in Fig.(1) with unequally spaced grid nodes for improving the accuracy and reducing the computational time. Computations were made over the circular-cross section in the plane of curvature and started at a position five diameters upstream of the bend.

2-2. Boundary Conditions

There are three different types of boundary conditions to specify the computational domain shown in Fig.(1): Inlet, outlet and wall boundary conditions. At the inlet, 5 diameters upstream the entrance of the bend, the axial velocity profiles were assumed as uniform profiles. While, a forced-vortex swirl velocity profile was assumed at inlet. On the other hand, the distribution of the turbulence kinetic energy, k, was assumed uniform. The rate of energy dissipation, ε, at the inlet section was estimated as a fixed length scale with the following expression,

$$\varepsilon_{in} = C_\mu \frac{k^{3/2}}{\ell} \qquad (5)$$

where, ℓ is the characteristic length scale of turbulence. At the outlet, the gradients of flow variables in the flow direction are zero ; $\frac{\partial \Phi}{\partial z} = 0$ (Neumann conditions), except the radial velocity v which is sit to zero. At the solid wall

boundaries, however, u = v = w= 0., i.e. no-slip conditions. The near wall total velocity, V_p (parallel to wall boundaries at a distance y_p), (where $V_p = \sqrt{u_p^2 + w_p^2}$ and subscript p gives the near wall node), could be correlated on similar lines of Blackshall and Landis[14]. The correlated universal velocity profile of Blackshall and Landis[14] was:

$$\frac{V_p}{V_\tau} = \frac{1}{\chi} Ln\left(Ey_p^+\right) \tag{6}$$

where V_τ and y_p^+ are the total friction velocity and the dimensionless wall distance defined respectively, by:

$$V_\tau = \sqrt{\frac{\tau_t}{\rho}} \quad , \quad y_p^+ = \frac{\rho y_p V_\tau}{\mu_t} \tag{7}$$

where τ_t is the total tangential shear stress at the wall, χ and E are the Von-Karman's constant and the roughness parameter given by Ref.[15].

$$\tau_t = \sqrt{\tau_w^2 + \tau_s^2} \tag{8}$$

where τ_w is the shear stress in the axial direction, r-θ plane and τ_s is the shear stress in the tangential direction, r-x plane

On a similar line of Ref.[13], the range of local equilibrium, near walls leads to:

$$V_\tau = C_\mu^{0.25}\sqrt{k} \tag{9}$$

$$\tau_t = \frac{\rho C_\mu^{0.25}\sqrt{k}}{\frac{1}{\chi} Ln\left(Ey_p^+\right)} Vp \tag{10}$$

The above formulation of wall function, equation (10) is multiplied by the factor $\cos(\beta_w) = \frac{u_p}{V_p}$ to obtain τ_w, where β_w is the angle between the total tangential velocity vector near the wall and the axial velocity vector, $\beta_w = \tan^{-1}(\frac{w_p}{u_p})$. The near wall dissipation rate can be deduced as, Ref.[13]:

$$\varepsilon_p = \frac{C_\mu^{0.75} k_p^{1.5}}{\chi y_p} \sqrt{\left[1 + j\frac{y_p}{y^j} Ln\left(Ey_p^+\right)\cos^2(\beta_w)\left\{j\frac{y_p}{y^j} Ln\left(Ey_p^+\right) - 2\right\}\right]_p} \tag{11}$$

This value is kept constant for near-wall points for straight walls as well as curved walls. Equations (9) to (11) give the values of k and ε at the nearest wall point (p) without solving the transport equations.

3. COMPUTATIONAL RESULTS AND DISCUSSION

The study of incompressible (air) and steady swirling-turbulent flow through 90 degrees bends with constant pipe diameter, D = 100 mm., was carried out numerically, Fig.(1). The effects of swirl intensity which is represented by the swirl angle (β), curvature ratio (δ), downstream tangent length (Zd) and Reynolds number (Re), on the performance of the bends were studied. A forced-vortex swirl velocity distribution is assumed at inlet. The study was performed to calculate the swirl flow characteristics in bends, such as longitudinal velocity (u), radial velocity (v), swirl velocity (w), static pressure (P), turbulence kinetic energy (k), pressure coefficient (C_p), skin friction coefficient (C_f) and bend loss coefficient (K_f) in the plane of bend-curvature. The flow characteristics through the bend were drawn at different stations. These stations were namely, at a plane half diameter upstream of the bend entry and designated as U-station and at 45 and 90 degrees along the bend and at plane eight diameters downstream of the bend exit. The studied Reynolds number were based on the inlet mean longitudinal velocity U_0 and the diameter of cross-section, D. The swirl intensity is measured by the swirl angle, β in degrees. The swirl angle is defined as the ratio between the near wall swirl velocity value at entrance to the upstream tangent and the inlet mean longitudinal-velocity.

3-1. Effect of Swirl Intensity on Flow Characteristics

The variation of flow parameters under the effects of different inlet swirl intensities are shown in Figs.(2) to (4). These effects are carried out for swirl intensities, β, of 0, 30, 45 and 60 degrees at Reynolds number of 1.38×10^4, bend curvature ratio of 0.1 and downstream tangent length of 10D. The developments of longitudinal velocity profiles through the bend as well as upstream and downstream tangents are shown in Fig.(2.a). The longitudinal velocity are normalized by the mean bulk velocity at entrance, U_0. It is clearly noticed that, in the case of zero-swirl intensity, the longitudinal velocity peak shifts towards the convex (inner) wall as the flow proceeds through the bend. The maximum value of longitudinal velocity increases as the flow moves through the bend while the longitudinal velocity decreases correspondingly near the concave (outer) wall. As a result, the u- profile is highly asymmetric. This is due to an unbalance between the radial pressure gradient and the centrifugal force inside the bend. In the present study, a uniform velocity profile is introduced at entrance. This causes a weak secondary flow and a velocity distribution in the inviscid central core is approximated to that of a free-vortex with a maximum value near the center of curvature of the bend. As the swirl component is introduced, another behavior is observed. A more flattened longitudinal velocity profiles are gleaned from the plot along the bend. As the flow proceeds through the bend, the presence of swirl could adjust the velocity profiles inside the bend to approach more symmetric than that of zero-swirl case. Moreover, the introduction of swirl can adjust the distortion caused in longitudinal velocity by the curvature effect. In general, the present effects of

swirl are in qualitative agreement with that of Anwer and So[5], So and Anwer[6] and Murakami and Kito[2]. It is noticed from Fig.(2.a) that the presence of swirl causes an added perturbation over that caused by bend curvature only. Therefore, the swirling flow cases require longer downstream tangent length for recovery, compared with that of without swirl case, Fig.(2.a). This is cleared also from Figs.(2.b) and (2.c), where a swirl velocity and high turbulence level in the downstream tangent are still found.

Supporting evidence of swirl flow domination through the bend and its downstream tangent at different locations is illustrated in Fig.(2.b). General features of swirl velocity distributions are found in Fig.(2.b). As the swirl intensity increases the swirl velocity peak is shifted towards the walls. For swirl angles of 45 and 60 degrees cases, the swirl velocity profiles behave like a solid-body rotation over the whole cross-section diameter. The w-profiles along the plane of curvature are symmetric at all stations, suggesting that the swirl center is coincide with the curved centerline of the bend. Furthermore, the behavior of w is increased linearly with the pipe radius in the core region and then decays to zero as approaching near walls. Thus, lending credence to the argument that the secondary flow in the cross-stream plane is dominated by a decaying superimposed solid-body rotation. This produces a very significant destabilizing effect on the flow in the viscous wall-layer. An important observation can be noticed in Fig.(2.b) is that, a rapid decay for stronger swirl through the bend. This can be explained as that the weak swirl does not interact very well with the bend curvature in contradiction with the strong swirl which is responded fastly with the bend curvature. A conclusion may be drawn here that the curvature of bend could accelerate the decaying of the intensive swirl flow than weaker swirl flow.

The profiles of turbulence kinetic energy are observed in Fig.(2.c) for all tested cases. The profiles are skewed towards the convex wall inside the curved bend for zero-swirl case. This is due to a higher longitudinal velocity gradient near the inner wall. These profiles, in general, are suppressed in the pipe core region compared to those computed for non-zero swirl cases. It is cleared that, as the swirl intensity increases, the turbulence energy is enhanced in the core region. For swirling flow in pipes, Anwer and So[16] indicated that rotation gives rise to the normal stresses. This rising can be explained as an additional turbulence production created as a result of extra strains. This additional production of turbulence is convected into the core and increases the turbulence level in the core region. Figure(2.c) shows also that the presence of swirl flow requires a long downstream tangent length to recover from the perturbation created by the bend curvature and the imparted swirl into the flow.

The wall static pressure distributions along the outer and inner walls and their downstream tangents are plotted in Figs.(3.a) and (3.b), respectively. The wall pressure distribution is defined as, $C_p = (P - P_{ref}) / 0.5\rho U_o^2$, where P is the wall pressure and P_{ref} is the reference pressure which is taken on the outer wall at the entrance of upstream tangent. The results for both zero-swirl and swirl

cases are assembled for comparison purpose. In these and other subsequent plots, $Z/D = 0$ is taken to be at the entrance to the inner curved-wall. Based on a mean radius of curvature of 5D, the plots of Figs.(3) and (4), have bend exit located at $Z/D = 7$.

Two points are immediately obvious from Figs.(3.a) and (3.b). Firstly, it can be seen that the slopes of the pressure drop curves in the downstream tangent for zero-swirl and swirl cases are essentially the same. Another point is that the wall static pressure drop increases in the presence of swirl. These observations are in agreement with that of Anwer and So [5] and Murakami and Kito [2]. This is due to increasing the friction losses as swirl intensity increases. In addition, the angular momentum decreases along the radius of curvature near the wall and the effect of streamline curvature is to enhance the turbulent mixing near the wall, as discussed previously. Therefore, low pressure coefficient is obtained due to the streamline curvature.

The skin friction coefficient is defined as, $C_f = \tau_t / 0.5\rho U_o^2$ and τ_t is the total wall shear stress produced by axial and tangential flows. Figures(4.a) and (4.b) indicate that, as the swirl intensity increases, the skin friction coefficient increases. In turn, it causes more pressure drop with increasing the swirl intensity. There are probably two main reasons for this behavior. First, the concave curvature has a destablizing effect and increases the skin friction coefficient. The opposite is true in the case of the convex wall. Second, the influence of an imposed swirl on two dimensional flows is confined to the wall region and then the skin friction coefficient created mainly from tangential shear stress, τ_s. It can be seen clearly also from Fig.(4) that, the rate of decreasing of the skin friction coefficient on the inner wall increases with increasing the swirl intensity. This is referred to the created pressure gradient inside the bend.

3-2. Effects of Geometrical Parameters and Inlet Conditions on Swirl Decay through Bends

The effects of curvature ratio, downstream tangent length and Reynolds number on swirl velocity distributions through bend and its downstream tangent are illustrated through Figs.(5) to (7), respectively. The swirl decay is represented by the parameter (S), which is defined as the ratio of the angular momentum over the cross-section to the inlet axial momentum. The effect of curvature ratio on the decay of swirl is shown in Fig.(5). It is noticed that, there is slower decay of swirl inside the bend as the curvature ratio increases. But, the process of the swirl decay is faster in the downstream tangent, i.e., as the curvature ratio increases, the swirl decay is fast in the downstream tangent, Fig.(5). The same conclusion was obtained by So and Anwer [6] for 180 degrees bend. It can be concluded that the curved bend could accelerate the decay of swirl in a pipe flow, and hence the flow was recovered from swirl and bend curvature immediately downstream the bend exit.

The results shown in Fig.(6) represent the swirl decay along the bend for different downstream tangents. As the downstream tangent increases, the decay of angular momentum is increased inside the bend, Fig.(6). On the other hand, there is a sharp decay after bend exit for shorter downstream tangent (Zd=10D). That is, because the flow approaches the end of short pipe fastly, and this causes a strong damping of swirl at the inlet of short downstream tangent through the elliptic nature of the flow.

Figure(7) shows that, the decay of swirl along the bend and its downstream tangent is reduced as the inlet Reynolds number increases due to increasing the axial momentum. It is also noticed that, the rate of swirl decay is less along the bend than that in the downstream tangent. Following the bend immediately, there is a rapid decay in the first part of downstream tangent pipe.

3-3. BEND-PERFORMANCE WITH SWIRLING FLOW

As a general conclusion, the swirl intensity, the curvature ratio, the downstream tangent length and the Reynolds number strongly affect the bend performance. The performance is measured by bend loss coefficient, K_f, where $K_f = \Delta P / 0.5\rho U_0^2$ and ΔP is the pressure drop across the bend. These effects are shown through Figs.(8), (9) and (10). It is seen that, with increasing Reynolds number, the bend loss coefficient decreases for all cases. Furthermore, the presence of swirl flow causes an increase in pressure drop, which increases as the swirl intensity increases, Fig.(8). Figure(9) shows that as the curvature ratio increases from 0.1 to 0.3, the value of the bend loss coefficient decreases. Furthermore, this coefficient increases with increasing the downstream tangent length as shown in Fig.(10).

To obtain a best performance of bend, carries an isothermal fluid regardless the uniformity the exit distributions of flow parameters, it is recommended that passing turbulent flow without swirl through the bend of short downstream tangent and high curvature ratio must be used. On the other hand, a long downstream tangent length, low curvature ratio bend and passing turbulent flow accompanied with high swirl intensity enhances the turbulence and pressure drop.

4. EXPERIMENTAL SETUP

4-1. Layout of the Experimental Apparatus

The layout of the experimental apparatus is shown in Fig.(11). Air flows through the pipe is provided by two screw-compressors. The compressed air is allowed to pass through the tested rig up to the downstream tangent, where it discharges into the atmosphere. The rate of air flow is controlled by using a control valve placed at a large distance upstream the swirl generator. Twenty-five static pressure tappings were drilled along the concave-wall, while, twenty-one were drilled along the convex-wall. The experiments were carried out in the test rig shown in Fig.(11). In this test rig, a bend with curvature ratio, (δ) of

0.216 is placed in the horizontal plane between upstream and downstream tangents. The internal diameter of all parts of the test rig is 100 mm. The length of downstream tangent is taken of 20 diameters after the bend exit.

The experiments were carried out to verify the present computational model. The longitudinal as well as the tangential (swirl) velocity distributions were measured along the radial direction in the plane of curvature. The longitudinal and swirl velocity profiles were measured across the plane A-A, Fig.(11), using a calibrated three-holes probe. The measurements were conducted at three stations along the tested bend. These stations are namely 3.24 diameters upstream of the bend entrance (station U), through the bend at station 45 degrees and 0.6 diameter downstream the bend exit (station Exit). The measurements of longitudinal and swirl velocities are conducted at a swirl angle of 45°. Furthermore, static pressure distributions were measured along the convex and concave walls of the bend. Also, wall static pressure distributions were measured along upstream and downstream tangent lengths. The wall static pressure distributions are measured using multi-tube manometers. The manometer fluid is water.

4-2. Swirl Generator

In the present experiments, the swirling motion of air is imparted to the axial stream using a swirl generator. Briefly, the swirl generator consists of six movable flat vanes. These vanes are guided into an ellipsoid hub. The vanes and the ellipsoid hub are inserted in a straight pipe of the same diameter of the bend-pipe and five diameters length. The system of the vanes and hub are connected to a movable ring on the outer circumference of the swirl pipe. This ring can be adjusted manually to adjust the required setting angle of vanes on the flow direction. So, small rotation of the ring gives constant setting angle of vanes. In the present experiments a constant setting angle of vanes is considered to give a constant swirl intensity during the experiments. The vanes setting angle can be varied from 0 to 90 degrees. However, the swirl generator is placed at nine diameters upstream the bend entrance. On the other hand, the swirl generator is replaced by a straight pipe of the same length and diameter of bend-pipe to perform the experiments for zero-swirl case.

4-3. Experimental Uncertainty

The most common source of errors is found in the total velocity (V) measurements. It comes mainly from the reading of head difference between the total and static pressure holes. In the present measurements, it is found that the maximum head difference gives error of 0.66% of total head. On the other hand, the minimum head difference gives error of 5.4% of total head. Furthermore, a 1-mm diameter pressure tap should introduce an error of less than 1% of dynamic-pressure compared with the ideal tap of 0.25 mm, Ref.[17]. Therefore, the average error in velocity measurements is about 1.74%.

5. EXPERIMENTAL RESULTS

Experiments are carried out at a pipe Reynolds number of 1.4×10^5. This corresponds to mean axial velocity, U_o, of 19.5 m/s. On the other hand, the swirler vanes are adjusted at a constant angle during all experiments, $\beta = 45$ degrees . The measurements of velocity, V, are conducted at three stations, namely at 3.24 diameter upstream of the bend, at $\theta = 45$ degrees inside the bend, and at bend exit. Furthermore, the yaw angle, α, of the probe is measured, from which u and w can be calculated through, $u = V \cos \alpha$ and $w = V \sin \alpha$.

Figure(12) shows the longitudinal velocity profiles, as measured at the three prescribed stations. It is observed a distorted velocity profile at station U. The longitudinal velocity profiles shown in Fig.(12), give an expected results of the introduction of swirl flow. With the swirl flow, the maximum longitudinal velocity occurs away from the bend centerline. The decrease of velocity profile in the central region is due to a core vortex. However, the core vortex cell created by swirl motion still affect the distribution of the longitudinal velocity up to bend exit, Fig.(12). It is explained as that, with the swirling velocity component, the flow inside the bend is pressed toward the wall. However, the strong swirl creates a very low-velocity in the core region. Consequently, the effective area for pressure rise is decreased. However, due to swirl decay inside the bend, the core vortex strength is reduced and hence, the distorted velocity region is reduced as the flow proceeds along the bend. To check the accuracy of velocity profiles measurements, the inlet and exit mass flow rates are calculated by integrating the measured velocity profiles over the inlet and exit cross-sections. It is found that the resultant error in the mass flow rate is about 0.5 % of the inlet mass flow rate.

The corresponding swirl velocity profiles at the same stations are indicated in Fig.(13). Figure(13) shows that the measured swirl velocity profile at the upstream is a linear function of radius over 70 % of the radius and the swirl is the solid-vortex type except at the bend wall regions. The maximum w occurs at 70 % of pipe radius at station U, while it reaches 85 % inside the bend (station 45). This is due to the interaction of swirl motion with the streamwise curvature of the bend. At the bend exit, the w-profile flattens out in the wall region. This leads to extra production of turbulence energy, but not necessarily to the existence of mean streamwise vorticity.

The results show that the outer wall pressure has a higher pressure than that of inner wall, Fig.(14). This is due to the centrifugal force created by the bend and swirl motion. Furthermore, the perturbation caused by the streamline curvature in the presence of swirl flow extends to the upstream of bend entrance. On the other hand, up to 5 diameters after bend exit, the distribution of pressure does not reach the straight pipe one. The latter effect is due to perturbation caused by the strong streamline curvature and swirl effects.

6. VERIFICATION OF COMPUTATIONAL RESULTS WITH EXPERIMENTS

To verify the present computational technique with the measured data, a computation process is carried out. However, the measured u and w profiles at station U is fed into the program with the specified geometry of the bend. Figures(15) to (19) indicate the comparisons between the present computational and experimental results. At station 45 degrees, there is some deviation between the computation and measurements near the central region and inner wall as shown in Fig.(15). This may be attributed to the unusual variation of pressure in the core vortex and vane losses when there is a swirl. In addition, the inability of k-ε model to capture this effect. With the stronger swirl, the overall curvature effect increases and the discrepancy between the predicted and measured velocity profiles are observed. Further, a fairly agreement is observed between the computational and experimental results of swirl velocity at the 45 degrees station, Fig.(16). Also, the comparisons shown in Figs.(17) and (18) for u and w, respectively give general agreements between the measured and computed profiles at bend exit. Finally, the pressure distributions give good agreement, Fig.(19).

7. CONCLUSIONS

The conclusions drawn from the present study are summarized below. It should be cautioned that they are only valid for 90-degrees smooth bends. The effects of swirl flow intensity, curvature ratio, downstream tangent and Reynolds number on the bend performance in the presence of swirl flow were studied. From the previous discussions, it can be concluded that:

(1) The standard k-ε model does not represent the general flow development accurately and overestimates the bend performance when the inlet flow has a strong swirl intensity. With the stronger swirl, the overall curvature effect increases and the discrepancies between the predicted and measured longitudinal velocity profiles are observed.

(2) Swirling flow through bends causes a strong perturbation after the bend exit. The effect is enhanced as the swirl intensity increases.

(3) The bend curvature could accelerate the swirling decay process in the case of the stronger swirl intensity than that of weaker swirl flow case. The small curvature bend with the long downstream tangent increases the decaying process of swirl velocity. Also, the introduction of swirl flow into a bend flow delays the recovery from bend curvature only.

(4) The swirling flow through mild - curvature bend requires a longer downstream tangent to attain the fully developed straight pipe flow. On the other hand, the opposite is found for small curvature bends.

(5) The decaying process of swirl inside the bend is fast by increasing the downstream tangent and reducing the inlet Reynolds number.

(6) Passing turbulent-isothermal fluid, without swirl through the bend of shorter downstream tangent and high curvature ratio causes small pressure drop. On the other hand the presence of swirl flow in lower curvature ratio bend with longer downstream tangent increases the pressure drop along the bend.

NOMENCLATURE

D	Pipe cross-section diameter, m.
G	Generation of turbulence kinetic energy, $kg/m/sec^3$
P	Static pressure, N/m^2.
r	Radial-coordinate measured from the center of curvature, m
Rc	Mean bend radius of curvature, m
Re	Pipe Reynolds number at entrance, $\frac{\rho U_o D}{\mu_\ell}$
u,v,w	Mean velocities along axial, radial and tangential (swirl) directions, respectively, m/sec
V	Mean-total velocity vector, m/sec
x	Tangential direction normal to the computational domain, m
y	Normal coordinate measured from the wall, m
y_p	Near-wall points distances, normal to the wall, m
z	Axial coordinate along the straight ducts, m
Zd	Downstream tangent length, m
Zu	Upstream tangent length, m

GREEK SYMBOLS

δ	Bend-curvature-ratio, $\frac{D}{2Rc}$
θ	Axial coordinate along the bend, degrees
μ_{eff}	Effective viscosity, $N.sec/m^2$
μ_ℓ	Laminar viscosity, $N.sec/m^2$
μ_t	Turbulent viscosity, $N.sec/m^2$
ρ	Density, kg/m^3

Subscripts

i	Inner wall
o	Outer wall and also, ,mean value

REFERENCES

[1] Shimizu, Y., "Flow and Loss of Multiple Bends", Dissertation, Nagoya University, 1975.

[2] Murakami, M., and Kito, O., "Effects of Swirling Flow Components on Discharge Coefficients of Elbow Flow Meters", Bull. JSME, Vol. 23, No. 175-7, Jan., 1980, PP. 43-50.

[3] Kitoh, O., "Swirling Flow Through a Bend", J. Fluid Mech., Vol. 175, 1987, PP. 429-446.

[4] Kitoh, O., and Yu, C. M. S., "An Analytical Solution to the Viscous Flows in Curved Duct with Inlet Swirl", Int. J. JSME, Vol. 38, No. 4, 1995, PP. 532-540.

[5] Anwer, M., and So, R. M. C., "Swirling Turbulent Flow Through a Curved Pipe", Part I:, "Effect of Swirl and Bend Curvature", Exp. Fluids, Vol. 14, 1993, PP. 85-96.

[6] So, R. M. C., and Anwer, M., "Swirling Turbulent Flow Through a Curved Pipe", Part II:, "Recovery from Swirl and Bend Curvature", Exp. Fluids, Vol. 14, 1993, PP. 169-177.

[7] Patankar, S. V., "Numerical Heat Transfer and Fluid Flow", McGraw-Hill, New York, 1980.

[8] Gosman, A. D., and Pun, W. M., "Calculation of Recirculating Flows", Rept. No. HTS /74/12, 1974, Dept. of Mech. Engg., Imperial College, London, England.

[9] Pratap, V. S., and Spalding, D. B., "Numerical Computation of Flow in Curved Ducts", Aeronaut. Q., Vol. 26, 1975, PP. 219-228.

[10] Bird, R. B., Stewart, W. E., and Lightfoot, E. N., "Transport Phenomena", Wiley, New York, 1960.

[11] Launder, B. E., and Spalding, D. B., "The Numerical Computation of turbulent Flows", Computer Methods in Applied Mechanics and Engineering, Vol. 3, March 1974, PP. 269-289.

[12] Leschziner, M. A., and Rodi, W., "Calculation of Annular and Twin Parallel Jets Using Various Discretization Schemes and Turbulence-Model Variations", Trans. ASME, J. Fluids Engg., Vol. 103, 1981, PP. 352-360.

[13] El-Askary, W. A. A. E., "Effect of Swirl on the Flow Characteristics through Curved Ducts", M. Sc. Thesis, EL- Menoufia University, Shebin EL-Kom, EGYPT, 1997.

[14] Blackshall, R. G., and Landis, F., "The Boundary-Layer Velocity Distribution in Turbulent Swirling Pipe Flow", Trans. ASME, J. Basic Engg., December 1969, PP. 728-734.

[15] Schlichting, H., "Boundary Layer Theory", Hemisphere McGraw-Hill, New York, Seventh Edition, 1979.

[16] Anwer, M., and So, R. M. C., "Rotation Effects on a Fully Developed Turbulent Pipe Flow", Exp. Fluids, Vol. 8, 1989, PP. 33-40.

[17] Goldstein, R. J., "Fluid Mechanics Measurements", Hemisphere Publishing Corporation, New York, 1983.

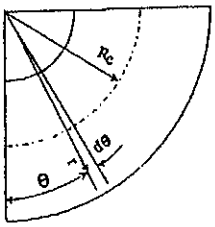

Bend Element and co-ordinates

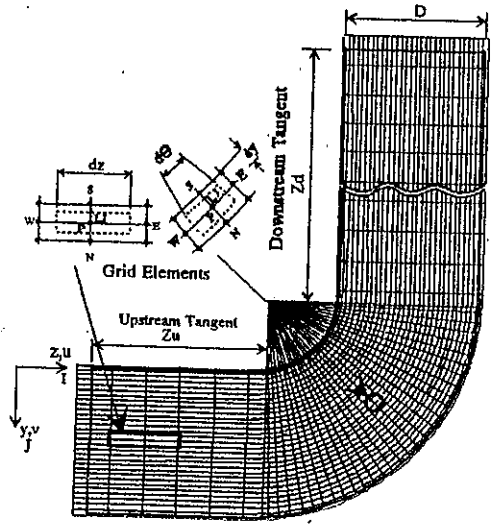

Fig.(1) Computational Domain of 90°-Bend

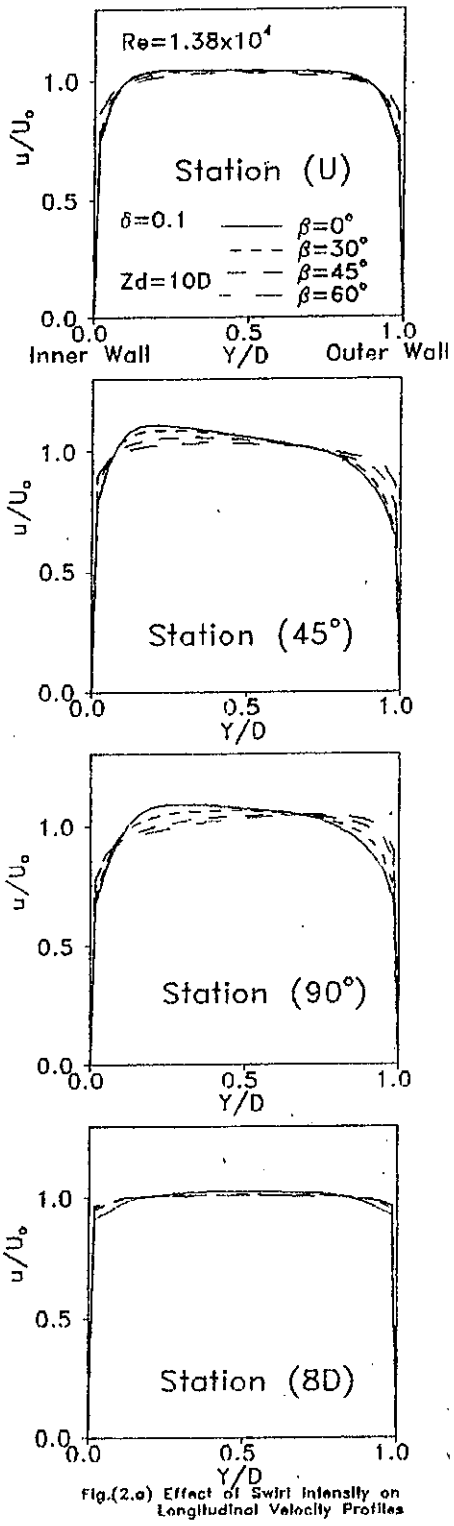

Fig.(2.a) Effect of Swirl Intensity on Longitudinal Velocity Profiles

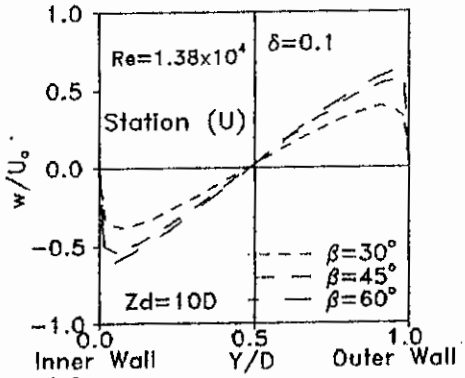

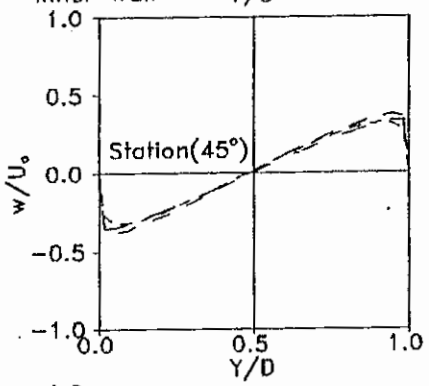

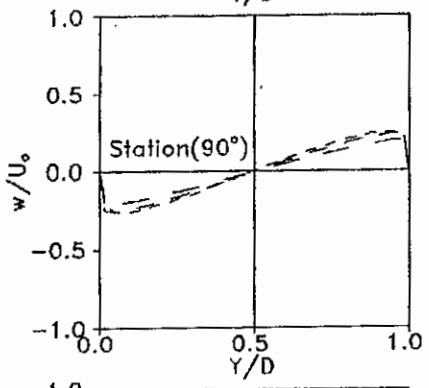

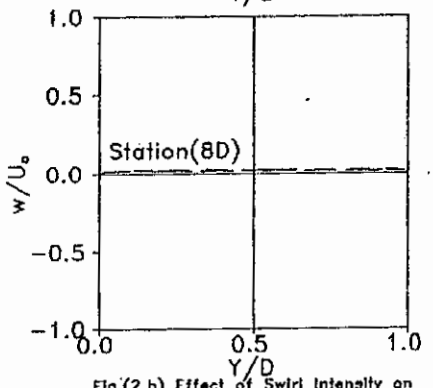

Fig.(2.b) Effect of Swirl Intensity on Swirl Velocity Profiles

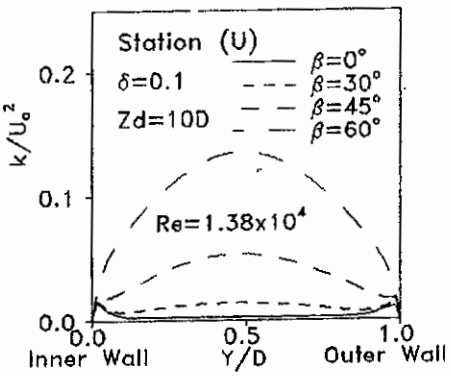

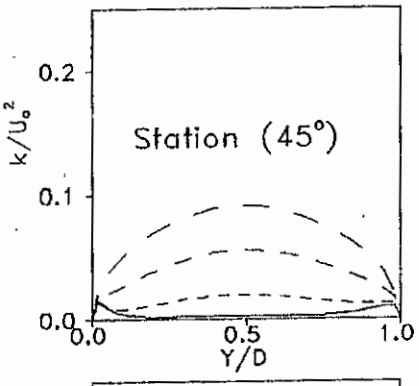

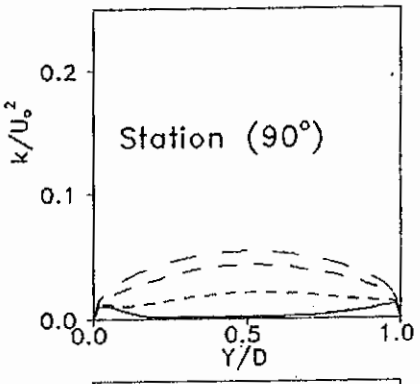

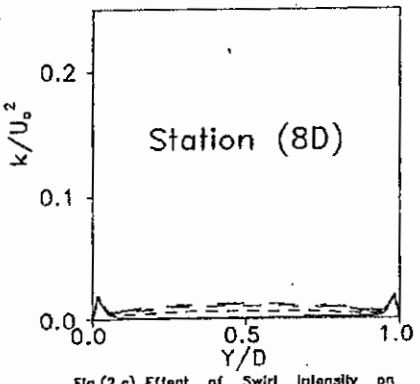

Fig.(2.a) Effect of Swirl Intensity on Turbulence Kinetic Energy Profiles

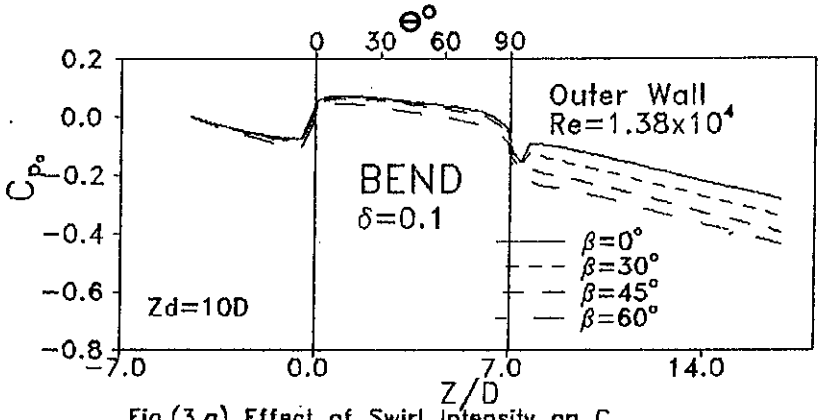

Fig.(3.a) Effect of Swirl Intensity on C_{p_o}

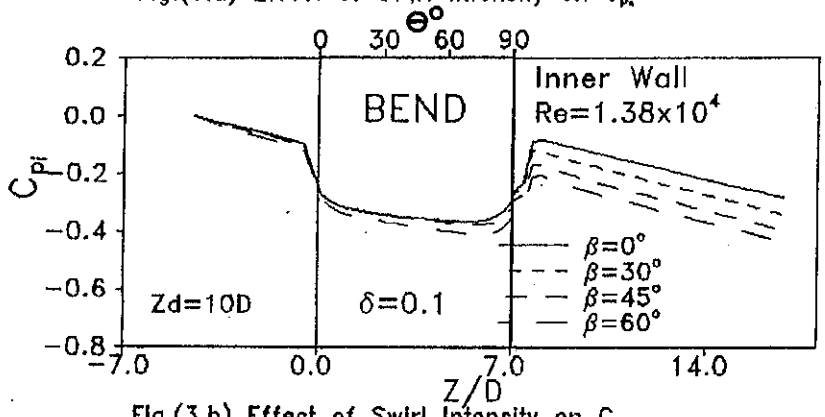

Fig.(3.b) Effect of Swirl Intensity on C_{p_i}

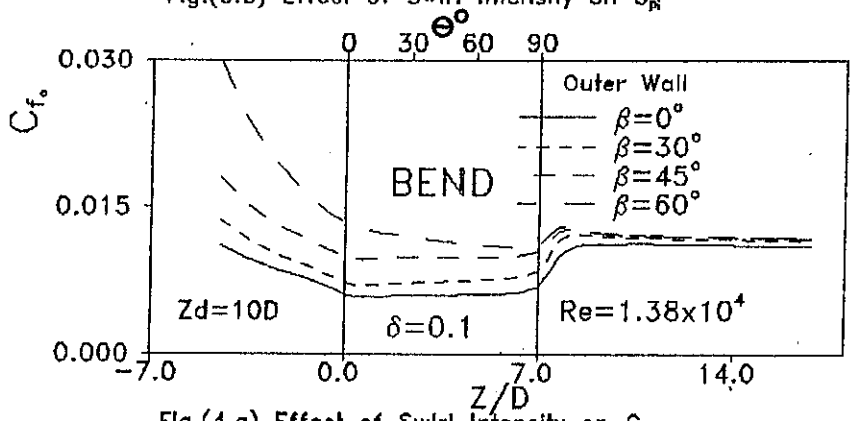

Fig.(4.a) Effect of Swirl Intensity on C_{f_o}

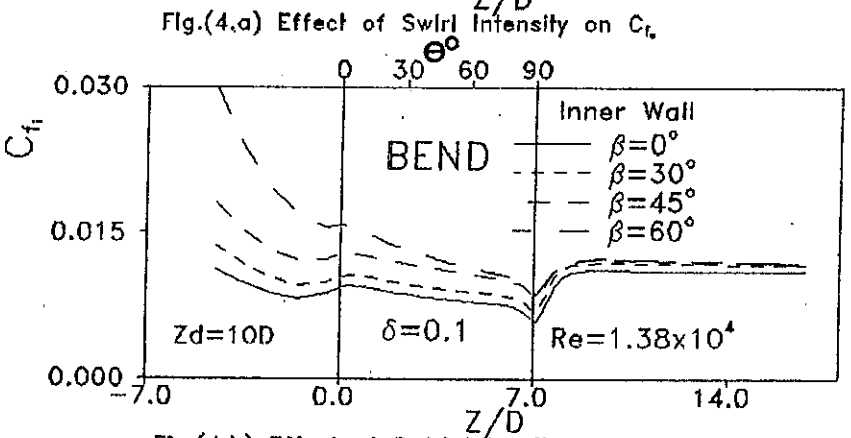

Fig.(4.b) Effect of Swirl Intensity on C_{f_i}

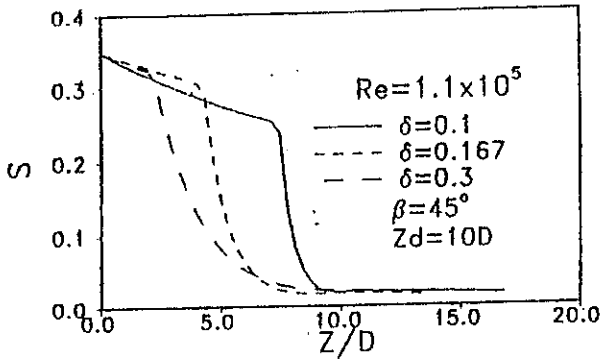

Fig (5) Effect of Curvature Ratio on the Decay of Angular Momentum (β = 45°).

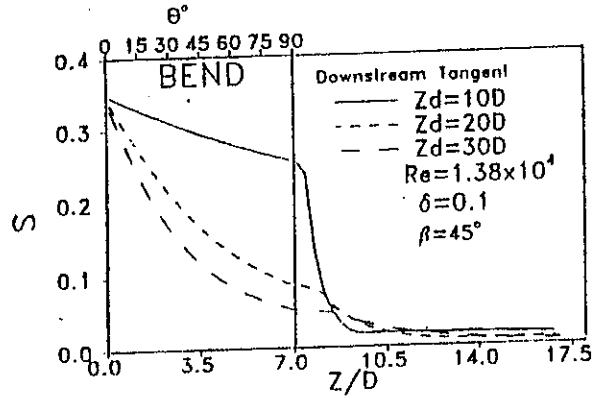

Fig (6) Effect of Downstream Tangent on the Decay of Angular Momentum (β = 45°).

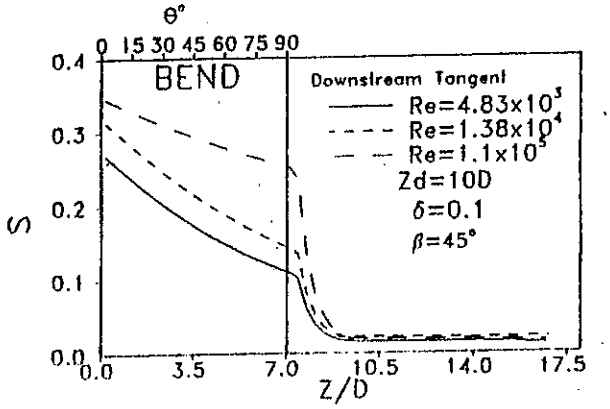

Fig (7) Effect of Inlet Reynolds Number on the Decay of Angular Momentum (β = 45°).

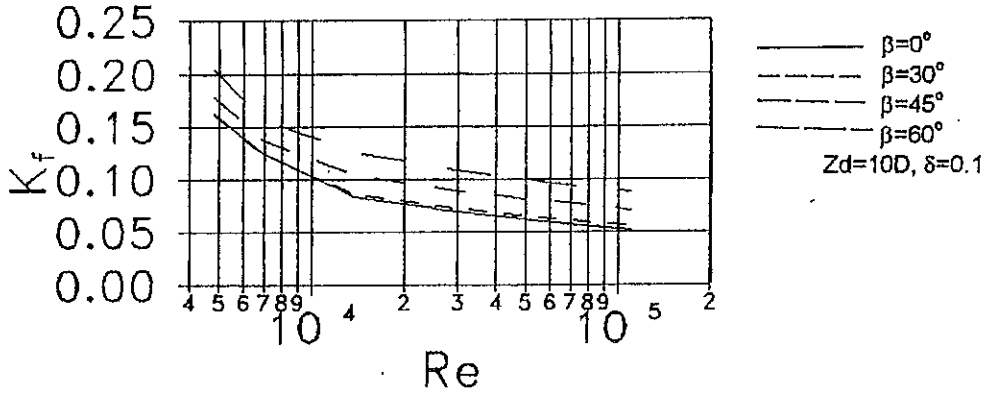

Fig.(8) Effect of Swirl Intensity on Bend Loss Coefficient

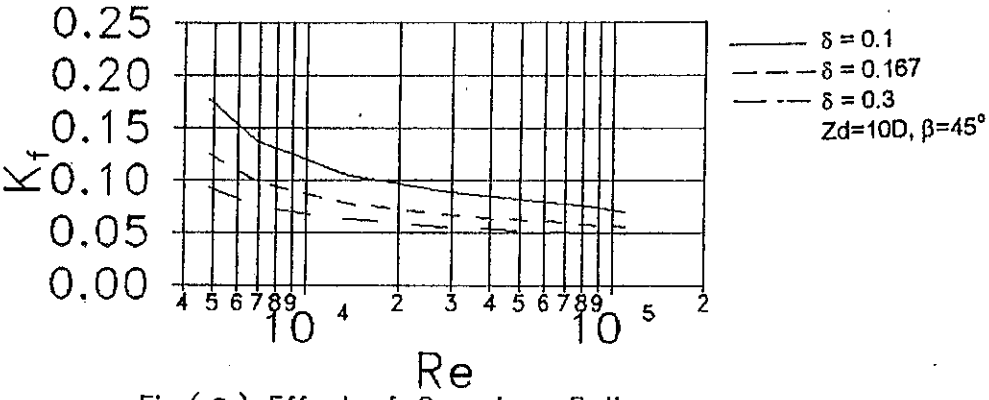

Fig.(9) Effect of Curvature Ratio on Bend Loss Coefficient (β=45°)

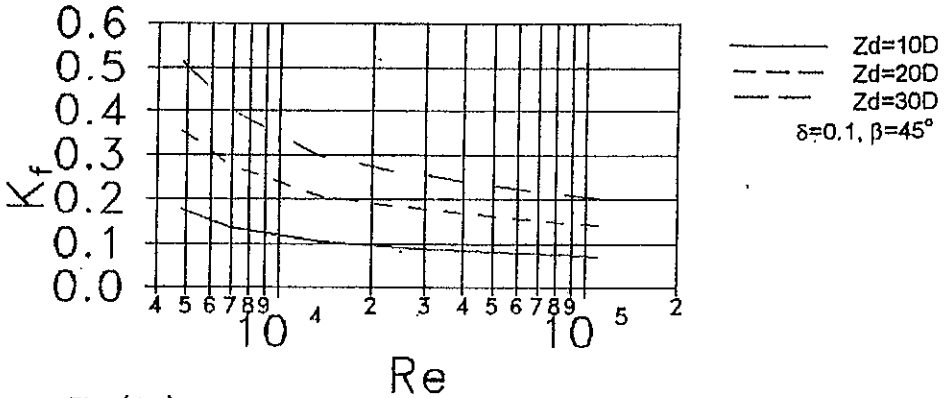

Fig.(10) Effect of Downstream Tangent on Bend Loss Coefficient (β=45°)

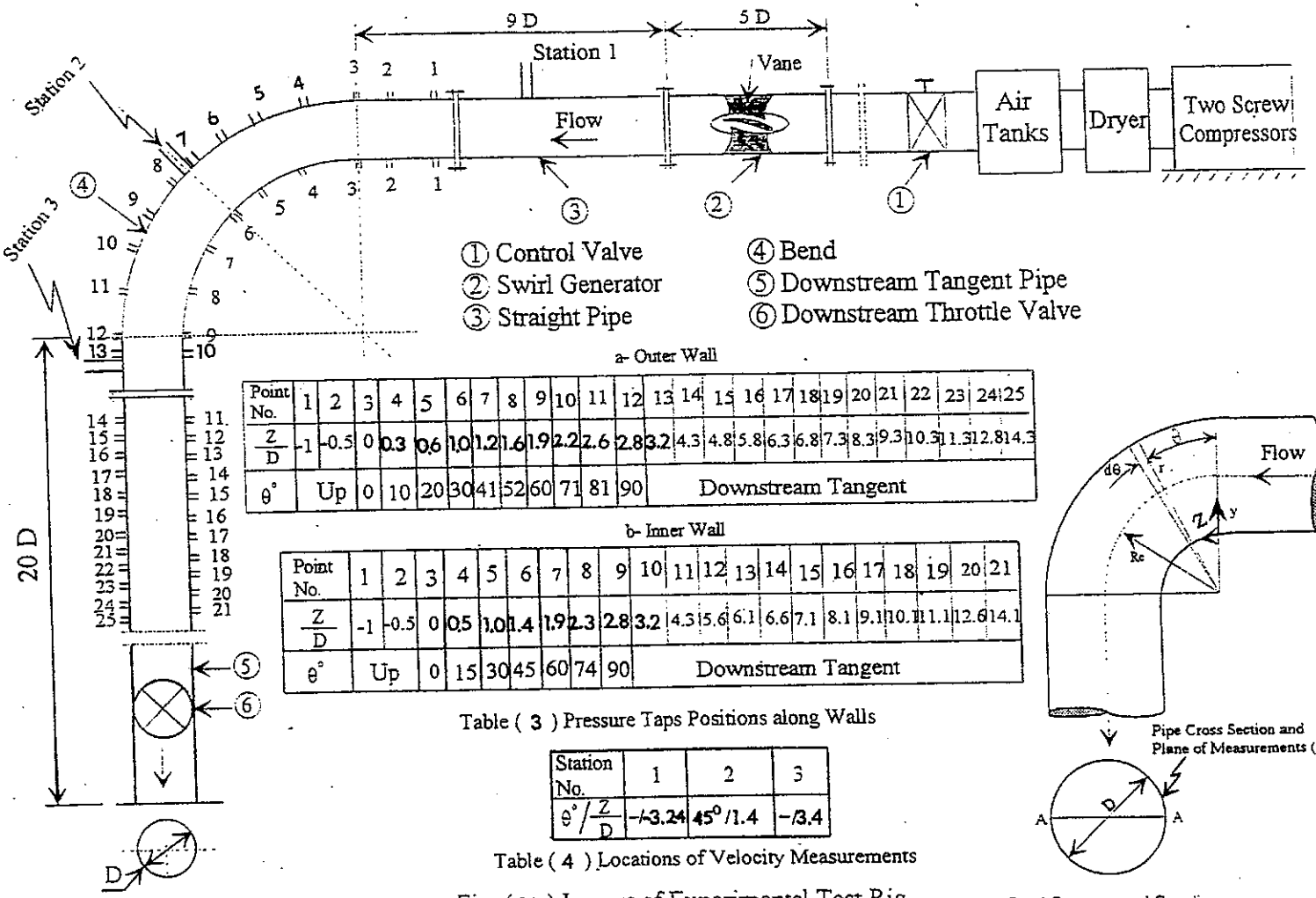

a- Outer Wall

Point No.	1	2	3	4	5	6	7	8	9	10	11	12	13	14	15	16	17	18	19	20	21	22	23	24	25
$\frac{Z}{D}$	-1	-0.5	0	0.3	0.6	1.0	1.2	1.6	1.9	2.2	2.6	2.8	3.2	4.3	4.8	5.8	6.3	6.8	7.3	8.3	9.3	10.3	11.3	12.8	14.3
θ°	Up		0	10	20	30	41	52	60	71	81	90	Downstream Tangent												

b- Inner Wall

Point No.	1	2	3	4	5	6	7	8	9	10	11	12	13	14	15	16	17	18	19	20	21
$\frac{Z}{D}$	-1	-0.5	0	0.5	1.0	1.4	1.9	2.3	2.8	3.2	4.3	5.6	6.1	6.6	7.1	8.1	9.1	10.1	11.1	12.6	14.1
θ°	Up		0	15	30	45	60	74	90	Downstream Tangent											

Table (3) Pressure Taps Positions along Walls

Station No.	1	2	3
$\theta^\circ / \frac{Z}{D}$	-/-3.24	45°/1.4	-/3.4

Table (4) Locations of Velocity Measurements

Fig. (11) Layout of Experimental Test Rig

Bend Geometry and Coordinates

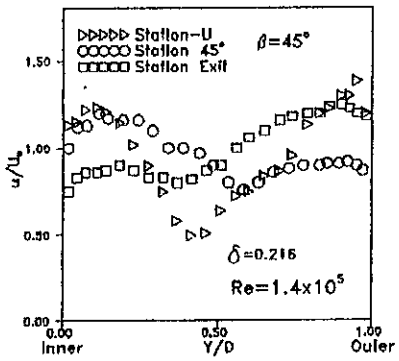

Fig.(12) Measured Longitudinal Velocity

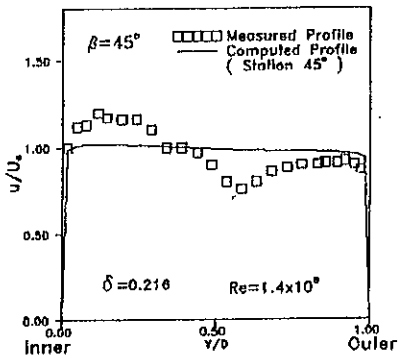

Fig.(15) Comparison Between Predicted and Measured Longitudinal Velocity

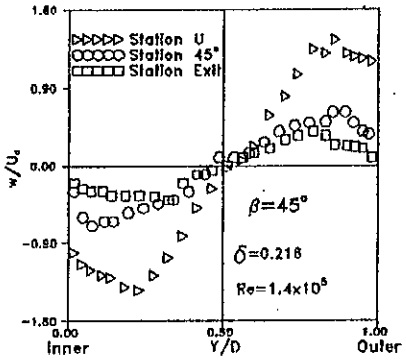

Fig.(13) Measured Swirl Velocity

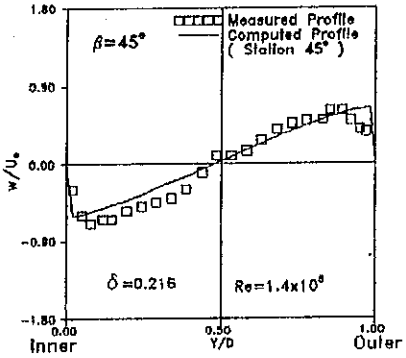

Fig.(16) Comparison Between Predicted and Measured Swirl Velocity

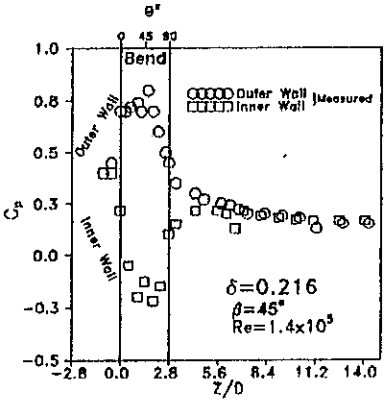

Fig.(14) Measured Wall Static Pressures

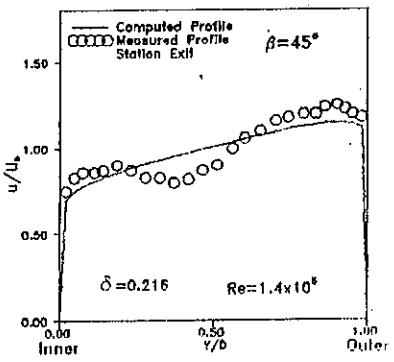

Fig.(17) Comparison Between Predicted and Measured Longitudinal Velocity

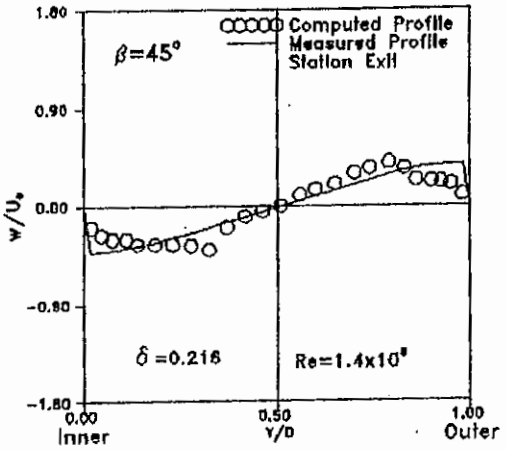

Fig.(18) Comparison Between Predicted and Measured Swirl Velocity

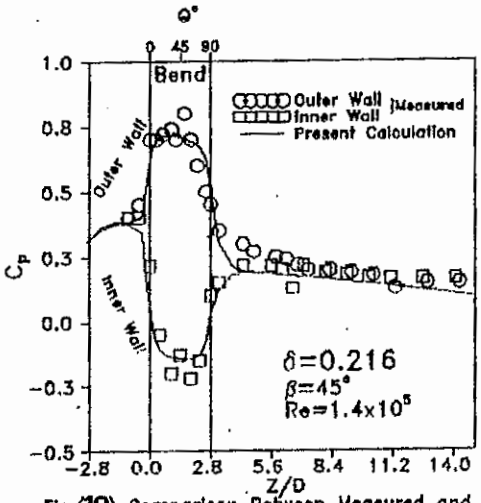

Fig.(19) Comparison Between Measured and Computed Wall Static Pressures

السريان الاضطرابى الدوامى خلال نفق منحنى ٩٠ درجة

فى هذا البحث يتم حساب خصائص السريان الاضطرابى الدوامى الغير قابل للانضغاط خلال مجرى منحنى بزاوية ٩٠ درجة، وذلك من خلال حل المعادلات الحاكمة (Navier-Stokes equations) واستخدام نموذج الاضطراب (k-ε). تم أخذ تأثير تقوس خطوط الانسياب فى الاعتبار وذلك لتحسين حسابات السريان الاضطرابى الدوامى خلال المجرى المقوس. كذلك تم فرض توزيع سرعة التدويم عند المدخل على اساس التدويم الجبرى. فى هذا البحث تم دراسة تأثير كلامن شدة التدويم، نسبة التقوس، طول النفق الخلفى وكذلك رقم الرينولدز على أداء المنحنى. كذلك تم دراسة تأثير التقوس على ظاهرة اخماد التدويم خلال النفق المنحنى. ولقد بينت النتائج النظرية مدى تأثير شدة التدويم عند المدخل على خصائص السريان خلال النفق المنحنى. من جهة اخرى فان معدل اخماد التدويم يتأثر بشدة بالبارمترات الهندسية للنفق المنحنى وكذلك حالة السريان عند المدخل. تم استخلاص نتيجة هامة من الدراسة النظرية وهى، يفضل استخدام نفق منحنى ذات نسبة تقوس كبيرة وطول نفق خلفى قصير فى ظل دخول سريان لايوجد به اى تدويم؛ وذلك من وجهة نظر الفقد فى الضغط. عموما، فأن وجود تدويم عند المدخل يزيد من الفقد فى الضغط والذى يزداد بزيادة شدة التدويم. تم عمل دراسة عملية ايضا وذلك للتحقيق من الدراسة النظرية. ولقد أظهرت المقارنة بين النتائج العملية والنتائج النظرية تحت نفس الظروف وجود توافق كمى ونوعى بينهما.